HMG Advance Access published October 6, 2013

Human Molecular Genetics, 2013 **1–11**
doi:10.1093/hmg/ddt455

Abnormal Ras signaling in Costello syndrome (CS) negatively regulates enamel formation

Alice F. Goodwin[1], William E. Tidyman[1,†], Andrew H. Jheon[1,†], Amnon Sharir[1], Xu Zheng[1,4], Cyril Charles[1,‡], James A. Fagin[5], Martin McMahon[2], Thomas G.H. Diekwisch[6], Bernhard Ganss[7], Katherine A. Rauen[2,3] and Ophir D. Klein[1,2,3,*]

[1]Department of Orofacial Sciences and Program in Craniofacial and Mesenchymal Biology, [2]Helen Diller Family Comprehensive Cancer Center and [3]Department of Pediatrics and Institute for Human Genetics, University of California, San Francisco, San Francisco, CA, USA [4]Department of Stomatology, Peking University Third Hospital, Bejing, China [5]Human Oncology and Pathogenesis Program, Memorial Sloan Kettering Cancer Center, New York, NY, USA [6]Brodie Laboratory for Craniofacial Genetics, College of Dentistry, University of Illinois at Chicago, Chicago, IL, USA and [7]Matrix Dynamics Group, Faculty of Dentistry, University of Toronto, Ontario, Canada

Received August 8, 2013; Revised and Accepted September 13, 2013

RASopathies are syndromes caused by gain-of-function mutations in the Ras signaling pathway. One of these conditions, Costello syndrome (CS), is typically caused by an activating *de novo* germline mutation in *HRAS* and is characterized by a wide range of cardiac, musculoskeletal, dermatological and developmental abnormalities. We report that a majority of individuals with CS have hypo-mineralization of enamel, the outer covering of teeth, and that similar defects are present in a CS mouse model. Comprehensive analysis of the mouse model revealed that ameloblasts, the cells that generate enamel, lacked polarity, and the ameloblast progenitor cells were hyperproliferative. Ras signals through two main effector cascades, the mitogen-activated protein kinase (MAPK) and phosphatidylinositol-3-kinase (PI3K) pathways. To determine through which pathway Ras affects enamel formation, inhibitors targeting either PI3K or MEK 1 and 2 (MEK 1/2), kinases in the MAPK pathway, were utilized. MEK1/2 inhibition rescued the hypo-mineralized enamel, normalized the ameloblast polarity defect and restored normal progenitor cell proliferation. In contrast, PI3K inhibition only corrected the progenitor cell proliferation phenotype. We demonstrate for the first time the central role of Ras signaling in enamel formation in CS individuals and present the mouse incisor as a model system to dissect the roles of the Ras effector pathways *in vivo*.

INTRODUCTION

The role of Ras signaling has been extensively studied in development and disease, particularly in cancer, yet its function in tooth development is not yet known. Receptor tyrosine kinase (RTK) signaling upstream of Ras is activated by fibroblast growth factors (Fgfs), which are known to regulate epithelial–mesenchymal interactions in the developing tooth (1). We have previously reported that deletion of Sprouty genes, which encode proteins that antagonize the Ras/mitogen-activated protein kinase (MAPK) pathway, results in changes in tooth number and morphology (2–4), suggesting that Ras signaling is important in developing teeth. However, the role of Ras and its downstream effectors, including the MAPK and phosphatidylinositol-3-kinase, (PI3K) pathways, has not yet been explored in tooth development and renewal.

Costello syndrome (CS) provides an ideal model to study the effects of activated Ras signaling in development. CS is characterized by craniofacial malformations, dermatologic anomalies, cardiac defects, musculoskeletal abnormalities, growth delay and cognitive deficits (5). CS is one of a number of RASopathies, a group of syndromes that include neurofibromatosis type 1

*To whom correspondence should be addressed at: University of California, San Francisco, 513 Parnassus Ave, HSE1509, San Francisco, CA 94143, USA. Tel: +1 4154764719; Fax: +1 4154769513; Email: ophir.klein@ucsf.edu
†Equal co-second authors.
‡Present address: Team 'Evo-Devo of Vertebrate Dentition', Institut de Génomique Fonctionnelle de Lyon, Ecole Normale Supérieure de Lyon, Université de Lyon, CNRS UMR 5242, Lyon, France.

© *The Author 2013. Published by Oxford University Press. All rights reserved.*
For Permissions, please email: journals.permissions@oup.com

Downloaded from http://hmg.oxfordjournals.org/ at University of Alabama at Birmingham on December 3, 2013

(NF1), Noonan syndrome (NS), NS with multiple lentigines, capillary malformation-AV malformation syndrome, Legius syndrome and Cardio-facio-cutaneous syndrome (CFC) (6). The RASopathies are caused by mutations that increase signaling through the Ras/MAPK pathway (6). In CS, individuals typically have heterozygous, *de novo* germline mutations in *HRAS* that result in the constitutive activation of Ras, although rarely somatic mosaicism in the parental germline has been reported as well (7, 8).

Multiple mouse models have been developed to study the RASopathies. Here, we have utilized a CS mouse model expressing a $HRas^{G12V}$ mutation (9). Although 80% of individuals with CS carry an $HRAS^{G12S}$ mutation (10–12), we utilized the available $HRas^{G12V}$ mouse model, which harbors the *HRas* mutation most commonly found in cancer, because it phenocopies many aspects of the syndrome, including growth delay, macrocephaly, craniofacial anomalies and papilloma development (9).

We examined the teeth of individuals with CS and in CS ($HRas^{G12V}$) mice and observed that enamel was hypo-mineralized in both human and mouse CS. Because human teeth no longer possesses ameloblasts since they slough off after crown formation is complete during tooth eruption, we cannot study amelogenesis or enamel formation in human patients. To systematically study the cellular mechanisms underlying the CS enamel defect, we took advantage of the continuously growing mouse incisor model (13–19). We discovered that in CS mice, the proliferation and differentiation of enamel-producing ameloblasts and their precursors were compromised, and the inhibition of MEK1/2 (MAPK) or PI3K rescued distinct aspects of the dental phenotype. Our studies demonstrate for the first time the central role of Ras signaling in tooth development, and the utilization of the mouse incisor model to dissect the roles of the distinct components of Ras signaling.

RESULTS

Individuals with CS have defective enamel

Enamel hypoplasia has been mentioned in case reports of CS individuals (20, 21), and here, we analyze the enamel defect of CS in a relatively large cohort of CS individuals. Because of the optical properties of enamel, less dense enamel appears to be chalky white and opaque to the human eye, whereas normal enamel looks translucent. Therefore, the presence of white lesions is suggestive of decreased enamel mineralization (22). The enamel of nearly all CS participants examined ($n = 29$; 88%) had focal white lesions and striations, which are not normally present in healthy enamel (Fig. 1A and B). In addition, pathologic wear, as indicated by reduced cusps and/or cup-shaped lesions on the cusps (Fig. 1C and D), was present in 56% ($n = 18$) of CS subjects. Such pathologic wear, not observed in unaffected individuals of the same age, suggested that CS individuals' enamel was less densely mineralized, and thus, more susceptible to abrasion (Fig. 1C and D). In order to increase the contrast between the mineralized and hypo-mineralized enamel areas, we obtained photographs using a UV camera, which confirmed that individuals with CS had hypo-mineralized striated lesions, seen as dark bands in the UV images, which were not present in controls (Fig. 1E and F).

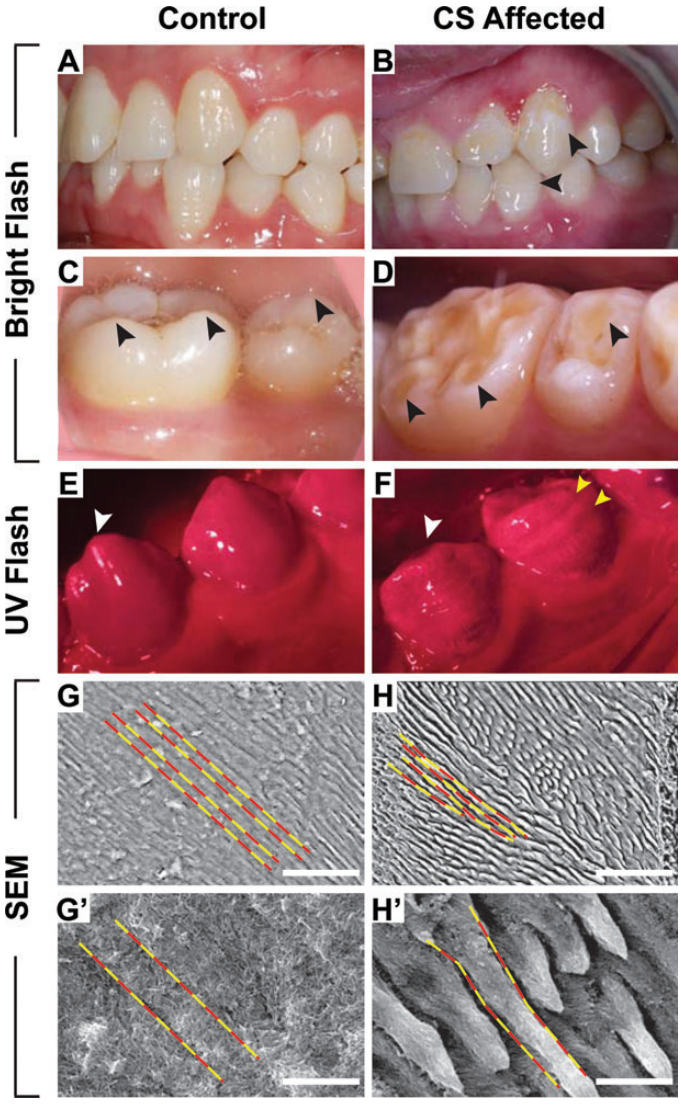

Figure 1. Defective enamel is a feature of CS. (**A**–**D**) Intraoral photographs. Control patient (A) had normal enamel, whereas 19-year-old affected female (B) had demineralized white spot lesions and striations (black arrows). Control patient (C) had normal cusps, whereas 23-year-old affected male (D) had cup-shaped lesions (black arrows) on cusps. (**E** and **F**) UV flash images of mandibular canine and first premolar in unaffected 15-year-old (E) and his 25-year-old CS affected brother with heavy wear on the cusps (F, white arrows). Alternating striations (yellow arrows) in (F) indicated demineralized enamel. (**G** and **H**) SEM images of enamel of exfoliated maxillary primary incisors showed that the hydroxyapatite crystals were less organized and not parallel in the affected CS individual (H) compared with control (G) as highlighted by the red and yellow dashed lines (scale bar: 50 μm). Higher magnification images showed that the inter-rod enamel present in the control (G′) was missing from the CS enamel (H′) (scale bar: 5 μm).

To assess for the presence of structural enamel defects, scanning electron microscopy (SEM) was performed on etched enamel from exfoliated CS and age-matched control teeth. Healthy enamel displayed a parallel arrangement of hydroxyapatite prisms spanning from the dentin–enamel junction (DEJ) to the enamel surface (Fig. 1G). In CS enamel, the organized, parallel pattern of hydroxyapatite prisms was absent, and the orientation of rods was more irregular from the DEJ to

Downloaded from http://hmg.oxfordjournals.org/ at University of Alabama at Birmingham on December 3, 2013

the enamel surface (Fig. 1H). More importantly, the inter-rod hydroxyapatite crystals that fill the space between enamel rods in normal enamel (Fig. 1G′) were absent in CS enamel (Fig. 1H′). Furthermore, micro-computed tomography (μCT) analysis of exfoliated primary teeth showed that the enamel in CS subjects was thinner than in controls ($n = 1$; Supplementary Material, Fig. S1).

CS (*Hras*^{G12V}) mice have poorly mineralized and disorganized enamel

μCT was performed on hemi-mandibles of CS (*HRas*^{G12V}) mice (Fig. 2A). Coronal images at the first molar were captured to determine the volume, distribution and density of molar and incisor enamel (Fig. 2A′). Normally, mice possess enamel on the crowns of the three molars and the labial aspect of the incisor (Fig. 2B, B′ and D, D′). However, the molars of CS mice showed little to no enamel (Fig. 2C, C″ and E, E″). In control mice, incisor enamel was more dense at postnatal day (P) 70 than P21 (Fig. 2B‴ and D‴). In fact, at all stages analyzed, the CS incisor enamel was less densely mineralized (Fig. 2C‴ and E‴). In controls, enamel covered the entire labial surface of the incisor, whereas in CS mutants, the total volume of enamel was decreased, with enamel covering a decreased percent of the surface area of the tooth (Fig. 2C‴ and E‴, Supplementary Material, Fig. S5).

To determine whether enamel microstructure was disrupted in CS mice, SEM analysis was performed on incisors of 12-week-old (P70) animals. In controls, the enamel rods were highly organized, running parallel in the same plane from the DEJ to the enamel surface (Fig. 2F and F′) similar to the pattern observed in human teeth (Fig. 1G). This interdigitated and highly organized pattern was lost in CS incisors, and the enamel rods intersected at irregular angles and did not completely span the DEJ to the enamel surface (Fig. 2G and G′), similar to what we observed in human CS teeth (Fig. 1H).

μCT imaging of CS mice also revealed large cysts in the bone in the region of the third molar at P21 when compared with control ($n = 3$; Fig. 2B and C). Histological examination of the cysts at P21 revealed that they were lined by epithelium infiltrated by ghost cells, or aneucleic cells with basophilic granules (data not shown). The cysts were near, but not associated with, the third molar, which is suggestive of calcifying odontogenic cysts (23). Interestingly, these cysts were not observed at P70, indicating that they resolved in adulthood ($n = 3$; Fig. 2E).

CS (*Hras*^{G12V}) ameloblasts are disorganized and have abnormal cell polarity at the secretory and maturation stages

In order to determine the cause of the enamel defects in the CS (*Hras*^{G12V}) mice, the ameloblasts were examined using the mouse incisor model. The rodent tooth is remarkable in that the ameloblast progenitor cells exit the stem cell-containing cervical loop (CL), proliferate as they move into the transit-amplifying (TA) region and differentiate into ameloblasts. As the ameloblasts move along the incisor, they transition from the secretory stage, during which they secrete enamel proteins including amelogenin (AMEL) and ameloblastin (AMBN) to form the enamel matrix (24, 25), to the maturation stage, when ameloblasts secrete proteins such as odontogenic ameloblast-associated protein (ODAM/APIN) and amelotin (AMTN) that enable the

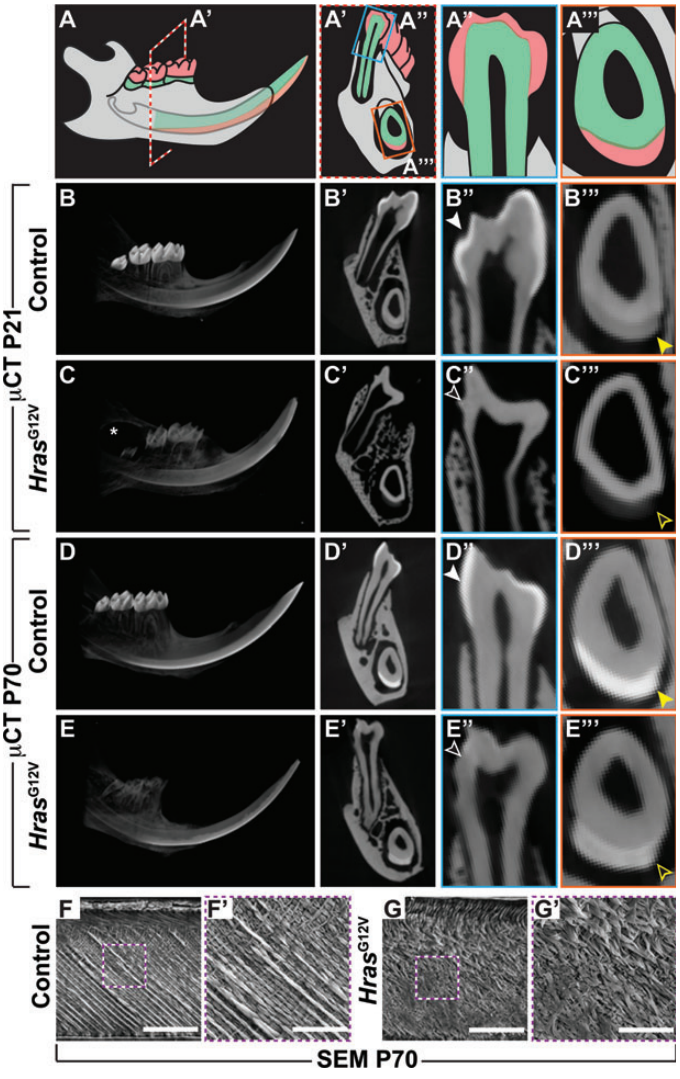

Figure 2. CS (*Hras*^{G12V}) mice have less densely mineralized, disorganized enamel. μCT images of the entire mouse mandible (**A**) and first molar and incisor (A′) (red dashed plane). (A′, A″) Magnified view of the molar and incisor. Enamel is colored red, dentin is green and bone is gray. (**B**–**E**) In control, enamel was present on the molars (B′,B″,D′,D″; white arrows) and labial aspect of the incisor (B′,B‴,D′,D‴; yellow arrows), while the CS mutant had little to no enamel on the molars (C′,C″,E′,E″; open white arrows) and less dense and abnormally distributed enamel on the labial aspect of the incisor at P21 (C′,C‴) and P70 (E′,E‴; open yellow arrows). Note the large cyst structure in the region of the third molar in the CS mutant (marked by an asterisk) at P21 (C) that was resolved at P70 (E). (**F** and **G**) SEMs showed that control enamel rods were parallel and ran continuously from the DEJ (bottom of image) to the enamel surface (top of image) (F′), while the CS mutant enamel rods were disorganized and intersected (G′) (scale bar: G,H; 50 μm G′,H′; 10 μm).

mineralization of the enamel matrix (26, 27). Thus, the distinct steps of amelogenesis can be observed in a 'conveyor belt-like' fashion along the length of the mouse incisor.

Normally, ameloblasts are highly organized in a single cell layer on the labial aspect of the incisor (Fig. 3A and A′). Hematoxylin and eosin (H&E) stained coronal sections in the region of the first molar from P70 control mice showed that the ameloblasts and underlying stratum intermedium (SI) cells were separated by a clear border (Fig. 3B and B′). In addition, control ameloblasts were polarized, with the nuclei located in the

Downloaded from http://hmg.oxfordjournals.org/ at University of Alabama at Birmingham on December 3, 2013

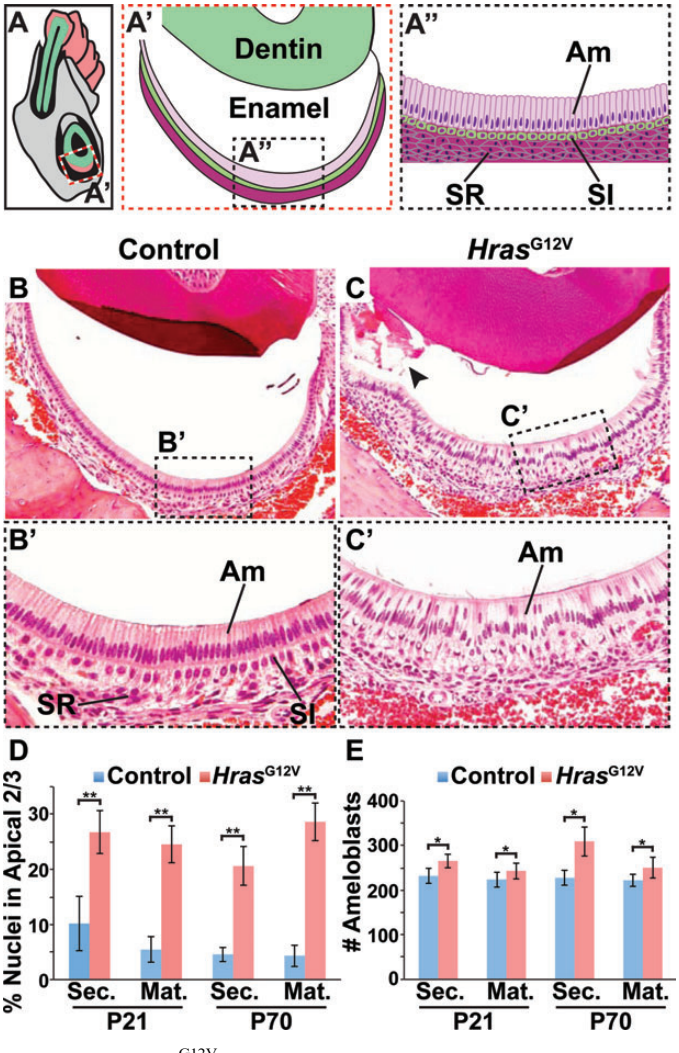

Figure 3. CS (*Hras*^{G12V}) ameloblasts are disorganized and lose cell polarity. Coronal sections of the mouse mandible at the plane of the first molar, as shown in **A**, were stained with H&E. Images were taken of the labial aspect of the incisor at 20× (A′) and 40× (A″). (**B**, B′) In control, the ameloblasts (Am) were highly organized, with their nuclei in the basal aspect of the cell, and there was a clear border between the ameloblasts and underlying SI and SR. (**C**, C′) In the CS mutant, the ameloblasts were crowded, the nuclei were in the apical 2/3 of cells, and there was no clear boundary between the ameloblasts and SI/SR. The enamel space in the control was empty (B), while there was pink stained enamel matrix protein (marked by the arrow) in the CS mutant (C). The percentage of nuclei in the apical 2/3 of the cell (D; $^{**}P < 0.0025$) and the number of ameloblasts in the labial aspect of the incisor (E; $^{*}P < 0.025$) at secretory (Sec.) and maturation (Mat.) stage are quantified. (Am, ameloblast; SR, stellate reticulum; SI, stratum intermedium).

basal portion of the cell (Fig. 3B and B′). In contrast, CS ameloblasts and the underlying SI and stellate reticulum (SR) were disorganized, and there appeared to be a loss of the well-defined border between ameloblasts and SI (Fig. 3C and C′′; (9)). CS ameloblasts appeared to be crowded (Fig. 3C′), and there was an increased number of CS ameloblasts at both the secretory and maturation stages (Fig. 3E). Furthermore, the nuclei in CS ameloblasts were located in the apical two-thirds of the cell significantly more often than in controls at both the secretory and maturation stages (Fig. 3B′, C′ and D). This mis-orientation of nuclei indicated a loss of cell polarity. In control ameloblasts, the Golgi apparatus is positioned apically with respect to the nuclei. However, in a significant number of CS ameloblasts, the Golgi apparatus was mis-oriented basally relative to the nucleus, demonstrating a lack of CS ameloblast polarity (Supplementary Material, Fig. 2). Interestingly, there were no differences between control and CS mice in expression of the hemi-desmosomal protein E-cadherin (28) or the desmosome-associated protein PERP that are important in ameloblast–SI attachment and necessary for proper enamel formation ((29); data not shown).

When ameloblasts reach the maturation stage, the enamel protein matrix is normally removed to allow proper mineralization (30). In demineralized samples from control mouse incisors, the empty enamel space between the ameloblasts and dentin confirmed the complete removal of enamel matrix (Fig. 3B). In contrast, CS mice showed residual enamel matrix, indicating that CS ameloblasts did not completely remove the enamel matrix to form properly mineralized enamel (Fig. 3C). Furthermore, qPCR showed that maturation stage molars at P11 expressed decreased levels of *Amtn*, *Apin*/*Odam* and *Klk4*, a gene encoding another maturation stage enamel protein (Supplementary Material, Fig. S3).

Treatment with MEK and PI3K inhibitors enhances enamel deposition in control mice

In order to determine through which effector pathway HRAS acts to regulate amelogenesis, mice were treated with MEK1/2 (PD0325901, Pfizer, New York, NY, USA) or PI3K (GDC-0941, Genentech, South San Francisco, CA) inhibitors. The systemic inhibition of the signaling pathways by the specific inhibitors was confirmed by performing western blot analysis on protein isolated from the liver (Supplementary Material, Fig. S4). We first tested the effects of these inhibitors in control adult (P70) mice. Of note, since we treated adult mice, only the enamel of the incisor which grows continuously throughout the lifetime of the animal was affected and not the molars since molar formation is completed around P14 and erupted mouse molars do not possess ameloblasts, like human teeth. Coronal μCT images showed that mice treated with MEK or PI3K inhibitors for 28 days had normal enamel density on the labial aspect of the incisor (Fig. 4A′, E′ and I′); however, the enamel formed earlier after treatment with either of the inhibitors compared with vehicle-treated control mice. In control mice, enamel was visible on the labial aspect of the incisor near the first molar, whereas enamel appeared to be near the second molar with MEK inhibition and near the third molar with PI3K inhibition (Fig. 4A, E and I). Although the timing of enamel deposition differed, the incisor enamel structure analyzed by SEM was the same with vehicle, MEK and PI3K inhibitor treatments (Fig. 4B, F and J).

MEK inhibition of CS (*Hras*^{G12V}) mice rescues the enamel defect

We next assessed the effects of the pathway-specific inhibitors in CS adult mutant mice. Treatment of CS mice with the MEK inhibitor rescued the density, patterning and structure of enamel, whereas PI3K inhibition only partially rescued the enamel density and had no effect on the patterning or structure of enamel. CS mice treated with the MEK inhibitor produced densely mineralized enamel that covered the entire aspect of

Downloaded from http://hmg.oxfordjournals.org/ at University of Alabama at Birmingham on December 3, 2013

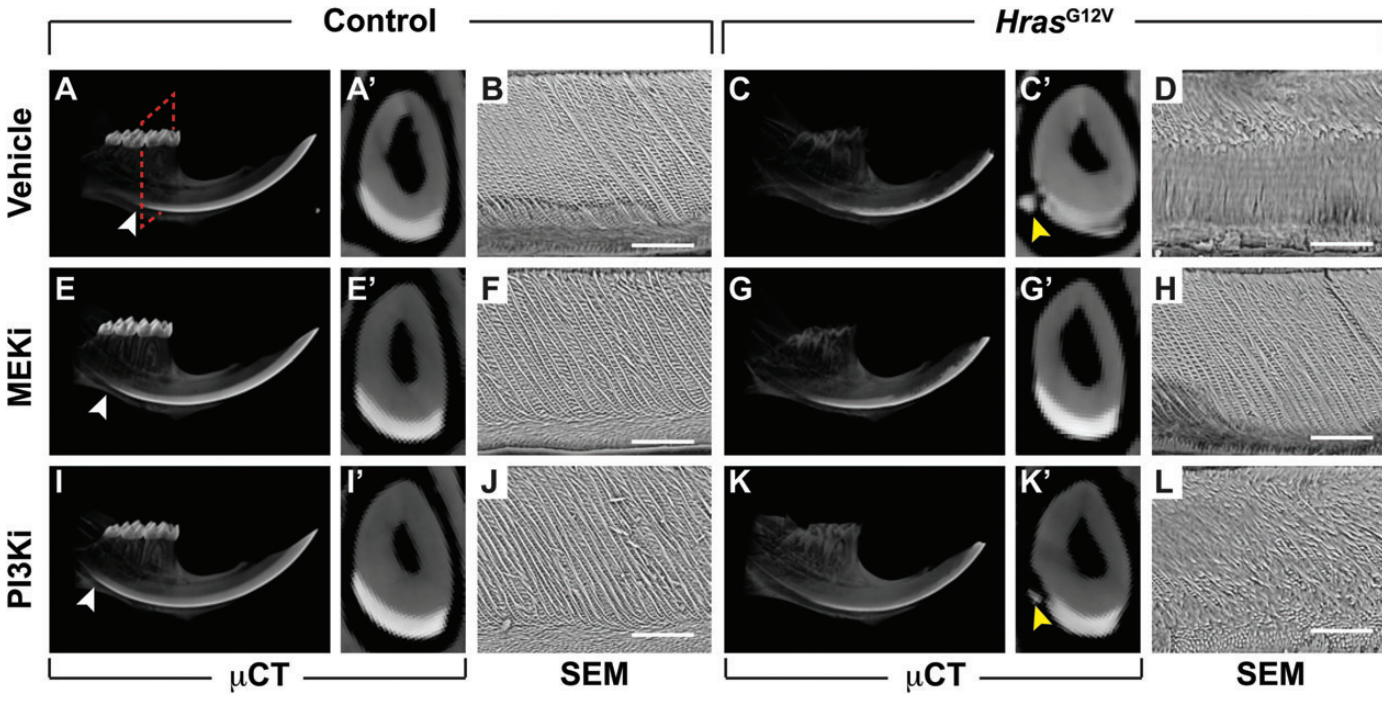

Figure 4. HRAS signaling negatively regulates enamel formation. Micro-CT (μCT) and SEM images of control and CS (*Hras*^{G12V}) incisors treated with vehicle, MEK1/2 inhibitor (MEKi) or PI3K inhibitor (PI3Ki) for 28 days. (**A**, **E** and **I**) Coronal μCT images of the incisor in the plane of the 1st molar indicated by the red dashed rectangle showed that enamel density and distribution was similar in control treated with MEKi (E′) or PI3Ki (I′) compared with vehicle (A′), but enamel mineralization began earlier as noted by white arrowheads. (**C**, **G** and **K**) The CS incisor treated with MEKi (G′) appeared to have denser enamel than the CS incisor treated with vehicle (C′) or PI3Ki (K′), similar to the control treated with vehicle (A′). Note MEKi (G′), but not PI3Ki (K′), treatment rescued CS enamel distribution pattern, including enamel pearl phenotype (marked by yellow arrowhead) (C′). (**D**, **H** and **L**) SEM images showed that the highly organized pattern of enamel rods in the control (**B**) was rescued in the CS incisor treated with MEKi (H), but not PI3Ki (L) (scale bar: 50 μm).

the labial incisor, similar to vehicle-treated control mice (Fig. 4A′ and G′). In fact, the enamel volume and percentage of tooth covered by enamel were not significantly different between MEK inhibitor-treated CS and vehicle-treated control incisors (Supplementary Material, Fig. S5). MEK inhibition not only rescued the density and patterning of enamel, but also restored the enamel microstructure comparable with the control (Fig. 4B and H). Treatment with a PI3K inhibitor resulted in the formation of enamel with slightly increased mineral density compared with CS enamel but less dense than control incisor, and thus, the rescue appeared to be less than with MEK inhibition (Fig. 4C′, G′ and K′). PI3K inhibition failed to rescue the distribution of enamel, as the enamel did not cover the entire labial aspect of the incisor, or the enamel structure, because the enamel rod pattern was disorganized similar to CS enamel (Fig. 4D and L). These studies using highly specific antagonists demonstrate that hyperactive HRAS signals primarily through MAPK to dysregulate enamel formation.

Underlying the rescue of the enamel mineralization defect was the normalization of the morphology of the enamel-producing ameloblasts. CS ameloblasts treated with the MEK inhibitor were normally polarized, with nuclei in the basal portion of the cell similar to control mice (Fig. 5A′, G′ and M). In contrast, PI3K inhibition did not rescue polarity of CS ameloblasts (Fig. 5D′, J′ and M). Also, in both vehicle-treated and PI3K-inhibited CS incisors, there was a residual enamel matrix in the enamel space (Fig. 5D and J). In 75% of samples, areas of sequestered enamel matrix were surrounded by disorganized ameloblasts (Fig. 5D) on the labial aspect of the CS incisor. These sequestered areas of matrix were presumably precursors of the enamel pearls, which are ectopic enamel spheres located primarily on the molars of human patients (31), observed on the lateral aspect of CS incisors treated with vehicle or PI3K inhibitor but not MEK inhibitor (Fig. 4C′, G′ and K′). In contrast, areas of sequestered enamel matrix were not observed in CS incisors treated with a MEK inhibitor, although they were present in incisors treated with a PI3K inhibitor (Fig. 5G and J).

MEK inhibition also appeared to rescue the ability of CS ameloblasts to differentiate and secrete enamel proteins. Ameloblast progenitors differentiate as they move along the incisor and secrete enamel matrix proteins once they have differentiated into ameloblasts. By measuring the distance from the CL to the start of expression of enamel proteins such as AMEL and AMBN, we can determine whether ameloblast differentiation is accelerated or delayed. In CS mice, there was an increase in the distance between the CL region and the appearance of the enamel protein AMEL compared with controls, suggesting that CS ameloblasts show a delay in enamel protein expression and thus have delayed differentiation (Fig. 5B, E and N). Treatment with a MEK inhibitor rescued this delayed expression, and CS ameloblasts began to secrete AMEL at the same location as control (Fig. 5H and N). In contrast, PI3K treatment of CS mice did not rescue the delay in the appearance of enamel proteins (Fig. 5K and N).

To determine differences in Ras/MAPK signaling in the CS incisor compared with control, p-ERK immunostaining was

Downloaded from http://hmg.oxfordjournals.org/ at University of Alabama at Birmingham on December 3, 2013

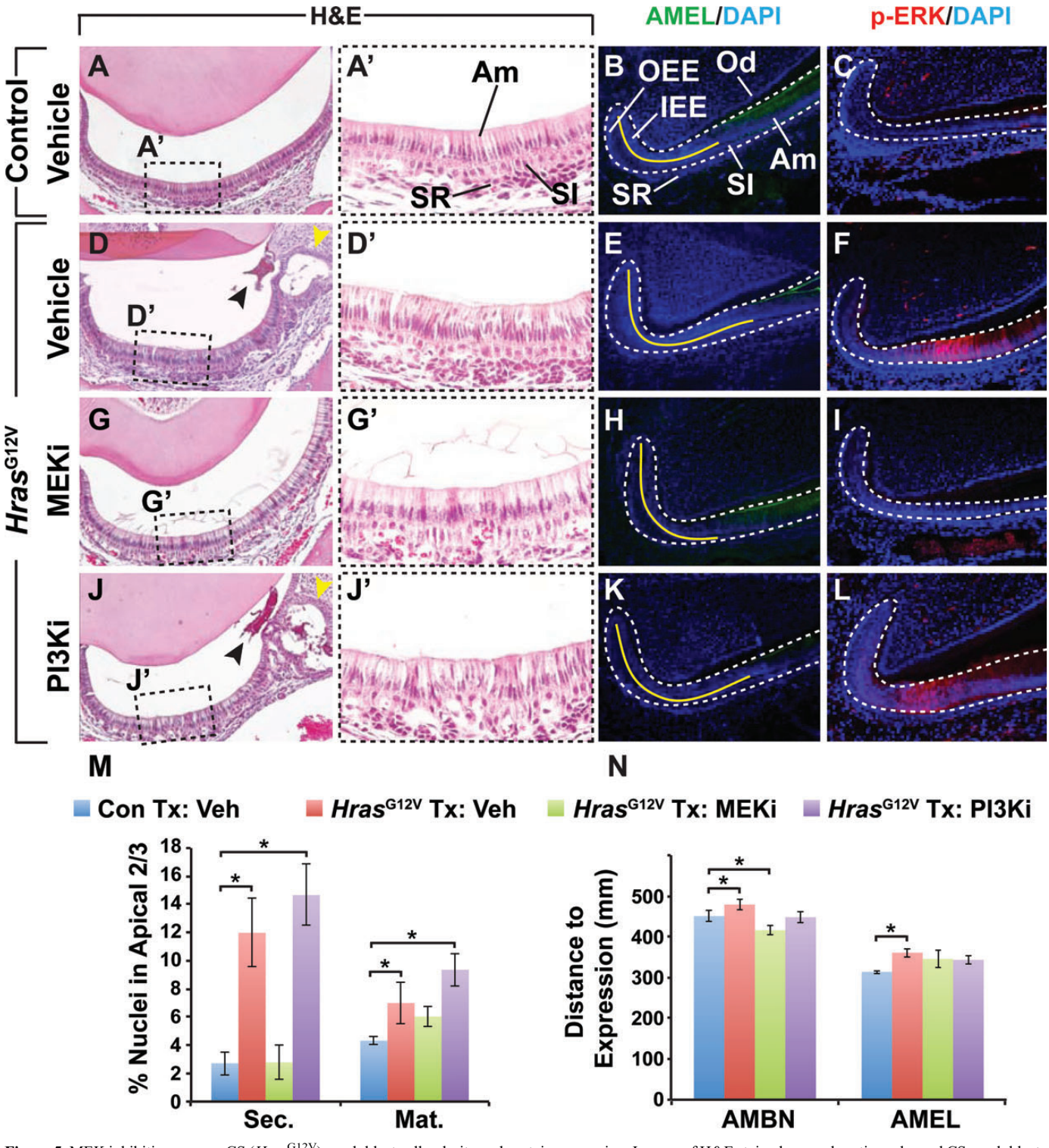

Figure 5. MEK inhibition rescues CS (*Hras*^{G12V}) ameloblast cell polarity and protein expression. Images of H&E stained coronal sections showed CS ameloblasts treated with the MEK inhibitor (MEKi) (**G** (20×), G′ (40×)) were polarized with nuclei in the basal portion of the cell, similar to control (**A**, A′), while the PI3′K inhibitor (PI3Ki) treated CS ameloblasts (**J**, J′) showed loss of polarity like the CS ameloblasts treated with vehicle (**D**, D′). Sagittal sections (20×) of mouse incisors stained with antibodies against amelogenin (AMEL) showed that expression of the secretory stage enamel protein was delayed and detected at a greater distance from the CL in CS incisor (**E**) compared with control (**B**). Treatment with MEKi (**H**) decreased the distance similar to control (B), unlike treatment with PI3Ki (**K**). Immunostaining on sagittal sections (20×) with an antibody against p-ERK showed high levels of expression along the length of the CS incisor (**F**) compared with control (**C**). Treatment of CS incisor with MEKi (**I**) reduced expression levels compared with that of control (C), while PI3Ki did not affect p-ERK expression (**L**). Quantification of the percentage of nuclei in the apical 2/3 of the ameloblasts (**M**; $^{*}P < 0.05$) and the distance from the CL to the start of enamel protein expression (**N**; $^{*}P < 0.05$) is shown in the graphs. (Am, ameloblast; SR, stellate reticulum; SI, stratum intermedium; OEE, outer enamel epithelium; IEE, inner enamel epithelium; Od, odontoblast; Sec, secretory; Mat, maturation; AMBN, ameloblastin).

Downloaded from http://hmg.oxfordjournals.org/ at University of Alabama at Birmingham on December 3, 2013

done. p-ERK expression in the control incisor was low compared with high levels of p-ERK activation along the length of the CS incisor (Fig. 5C and F). MEK inhibitor treatment of the CS incisor decreased the p-ERK levels to control, and PI3K inhibition did not affect p-ERK expression in the CS incisor (Fig. 5I and L).

MEK or PI3K inhibition rescues the hyperproliferative progenitor phenotype in CS (*Hras*^{G12V}) mice

The increase in ameloblast number at the secretory and maturation stages in CS mice was correlated with increased proliferation of progenitor cells in the CL and TA region compared with control (Fig. 6B and C). In the CS mouse CL/TA region, 25% of cells were proliferative, compared with 12% of cells in control mice (Fig. 6B, C and H). In addition, the length of the TA region was significantly shorter in CS mice compared with controls (Fig. 6B, C and I). In control mice, MEK and PI3K inhibition decreased proliferation in the CL/TA and decreased the length of the TA region significantly (Fig. 6B, D and F). There was no significant difference in proliferation or TA zone length between MEK- and PI3K-treated control mice (Fig. 6H and I). MEK inhibition of CS mice rescued the hyperproliferative phenotype, reducing proliferation to levels observed in control mice (Fig. 6B and E). However, the length of the TA region was not rescued (Fig. 6I). PI3K-treated CS mice showed reduced proliferation levels even below that of controls (Fig. 6B and G), and the TA region was significantly shorter than vehicle-treated control and CS mice (Fig. 6I).

DISCUSSION

The RASopathies are a group of syndromes estimated to affect 1 in 1000 live births. There are numerous morbidities associated with these syndromes, and presently, effective therapies are lacking. Although the role of Ras signaling has been studied in the development of several organs, almost nothing is known about its role during tooth development and renewal. Our analyses of both humans with CS and a CS mouse model revealed that activated HRAS negatively regulates enamel formation. Specifically, CS individuals with activated Ras signaling presented with hypo-mineralized, disorganized enamel, and a similar enamel phenotype was observed in CS mice. CS ameloblast progenitor cells were hyperproliferative, and CS ameloblasts lacked cell polarity. Furthermore, attenuation of the MAPK pathway led to the rescue of the enamel and ameloblast phenotypes, whereas modulation of either MAPK or PI3K signaling prevented progenitor cell hyperproliferation in CS mice.

The role of RTK, and particularly Fgf, signaling has been studied previously in tooth development, but the focus has been on tooth morphogenesis. Only a few studies have explored Fgf signaling in enamel formation, and thus, little is known about the role of RTK or downstream Ras signaling in enamel formation. Inactivation of *Fgfr1* in the epithelium resulted in dysfunctional ameloblasts that produced disorganized enamel (32). Overexpression of *Fgf2* in cultured embryonic molars resulted in decreased expression of amelogenin, while inhibition of FGF2 increased amelogenin expression and enamel formation (33). Interestingly, other Ras superfamily members have been shown to play a role in amelogenesis, including Rac, a GTPase involved in cytoskeletal remodeling that is directly activated by PI3K (34). Conditional inactivation of *Rac1* in the epithelium resulted in ameloblasts that expressed decreased levels of

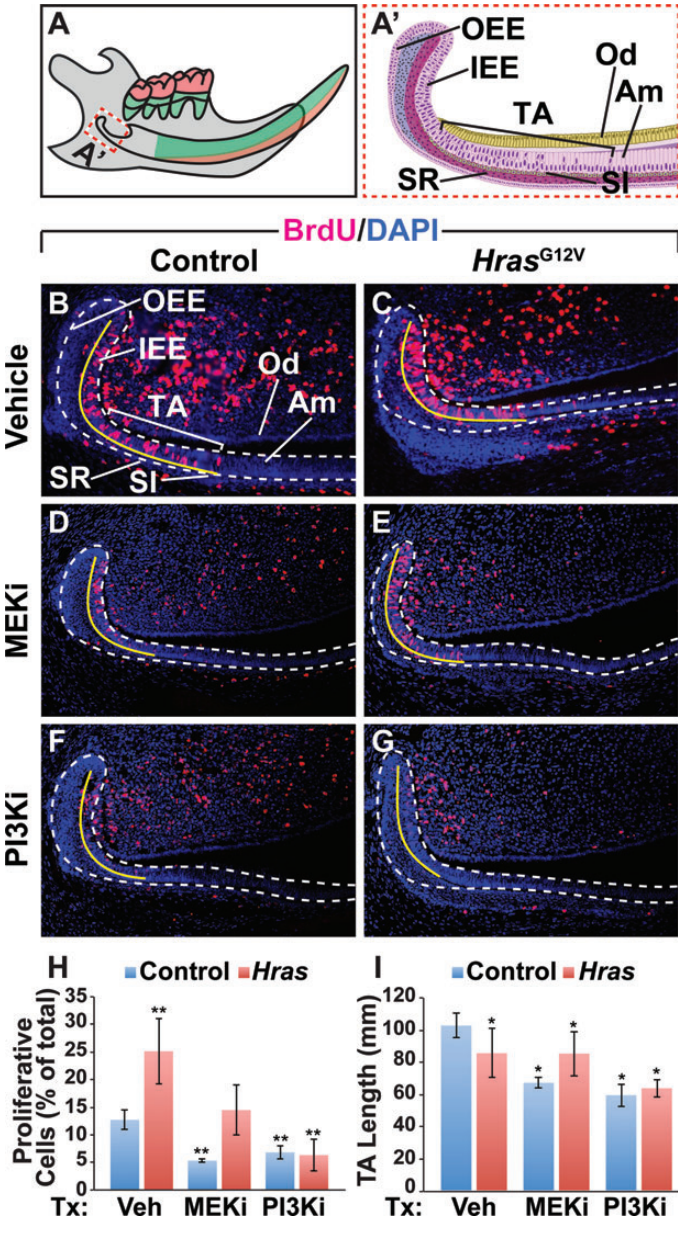

Figure 6. MAPK or PI3K inhibition rescues progenitor cell hyperproliferation in CS (*Hras*^{G12V}) mouse incisor. Immunostaining with an anti-BrdU antibody (red) and DAPI (blue) counterstain in the CL (A′ (20×)) at the proximal end of the incisor (**A**) revealed an increase in the number of proliferative cells in the CS incisor (**C**) compared with control (**B**) in the CL and transit amplifying (TA) region (outlined by the white dashed line). Proliferation was decreased in the control by treatment with MEK1/2 (MEKi) (**D**) and PI3K (PI3Ki) inhibitor (**F**), and the length of the TA zone was shortened (labeled with yellow line). Treatment of CS mice with MEKi (E) decreased the proliferation to control levels, and treatment with PI3Ki (**G**) reduced it below control levels; however, treatment with neither MEKi nor PI3Ki rescued the TA region length. The percentage of BrdU-positive cells (**H**; $^{**}P < 0.01$) and TA length (**I**; $^{*}P < 0.05$) are quantified in the graphs (significant compared with vehicle-treated control). (Am, ameloblast; SR, stellate reticulum; SI, stratum intermedium; OEE, outer enamel epithelium; IEE, inner enamel epithelium; Od, odontoblast; TA, transit amplifying region).

Downloaded from http://hmg.oxfordjournals.org/ at University of Alabama at Birmingham on December 3, 2013

amelogenin and lost attachment to the secreted enamel matrix, resulting in hypo-mineralized enamel (35). Thus, it is possible that activated HRAS disrupts Rac1 signaling, which may result in ameloblast dysfunction and hypo-mineralized enamel in CS.

Ras is thought to play an important role in cell polarity, proliferation and differentiation, but studies to address the mechanistic role of Ras signaling in cell biology have largely been performed *in vitro*. For example, tissue culture studies have shown that activation of KRAS and BRAF in a colon cancer cell line perturbs the polarity of cyst structures (36), and activation of HRAS in neuronal cell culture causes loss of polarity and multiple axon formation (37). Downstream of Ras, PI3K signaling has been shown to localize Rac and Cdc42 to the leading edge of cells undergoing chemotaxis to induce actin polymerization there (38), and in breast epithelial tumor cells, PI3K activates Rac, which results in loss of polarity (39). Only recently have investigators begun to study the role of Ras in cell polarity *in vivo*. A recent study showed that ERK controls spindle orientation during cell division in the developing lung (40). In our study, the loss of ameloblast polarity in CS mice was rescued by treatment with MEK but not PI3K inhibition, suggesting that, in the incisor, hyperactive Ras disrupts ameloblast polarity through MAPK. The mechanistic role that Ras plays in epithelial cell polarity is still unclear, and ameloblasts may serve as a useful model to further understand the role of Ras in the establishment and maintenance of epithelial cell polarity *in vivo*.

In vitro studies have shown that p-ERK and p-AKT regulate proliferation by decreasing $p27^{kip1}$ and $p21^{cip1}$ levels to allow progression from G_0 to S phase (41, 42). In the CS mouse incisor, proliferation in the CL and TA region was increased. MEK inhibition reduced proliferation to control levels, and PI3K inhibition reduced it even further. Thus, both MAPK and PI3K signaling are important in proliferation, and in CS, PI3K may have a larger role than MAPK in proliferation. Ras may also play a role in cell differentiation, as in the case of a $Nf1^{-/-}$ mouse model, in which increased differentiation of neuroblasts into glial cells was observed, and the increased differentiation was rescued by inhibiting ERK (43). We found that p-ERK levels were high in the CS incisor compared with the low levels in control incisors, indicating that a low level of p-ERK may be necessary for the ameloblast progenitors to exit the cell cycle and differentiate. MEK inhibition rescued the delay in ameloblast differentiation in CS mice and thus, in the CS mutant, consistently high levels of p-ERK result in hyper-proliferative progenitor cells and delay in ameloblast differentiation.

A number of inhibitors have been developed to target Ras and its effectors to treat cancer (reviewed in 44). These same inhibitors are potentially useful for treating RASopathies (45), and our study is the first to report modulation of the Ras pathway with inhibitors in CS. This concept has recently been explored in animal models of other RASopathies. For example, treatment of neurofibromatosis type 1 (NF1) mouse models with an MEK inhibitor (PD0325901) reduced the growth and proliferation of neurofibromas (46) and abrogated the myeloproliferative disease in these mice (47). In a NS mouse model with an activating mutation in *SHP2*, MEK inhibition with U0126 ameliorated craniofacial defects and rescued skull shape and size (48), and in another SOS gain-of-function NS mouse model, treatment with a MEK inhibitor (PD0325901) reduced embryonic lethality and rescued heart defects (49). A CFC zebrafish model expressing a kinase-activating $BRAF^{Q257R}$ allele or kinase-inactivating $BRAF^{G596V}$ allele developed craniofacial anomalies, and moreover, these defects were ameliorated by treatment with low doses of a MEK inhibitor at early stages of development (50). Interestingly, these studies focused on the role of MAPK signaling in NF1, NS and CFC, and very little work has been done to examine PI3K/AKT signaling in any of the RASopathies.

By comparing the distinct dental phenotypes found in the various RASopathies, we can obtain further insights into the role of the Ras pathway in human teeth. For example, whereas activating mutations in HRAS cause CS, individuals with CFC harbor activating mutations in the kinases BRAF, MEK1 or MEK2, which function downstream of HRAS (51, 52). Our inhibitor studies in the CS mouse model revealed that modulating the MAPK pathway rescued the enamel phenotype, which would suggest that CFC individuals with activating mutations in the MAPK pathway would have an enamel defect. However, in contrast to the enamel defects in CS individuals, CFC enamel appeared to be clinically normal (53), and SEM data showed that the structure of CFC enamel was normal (data not shown). Thus, increased Ras signaling in CS versus hyperactivation of MAPK signaling in CFC individuals has different effects on cells in the developing tooth, and whether this is due to quantitative differences in the levels of signaling or to qualitative differences in signaling outputs will be important future topics to explore. Data from clinical studies of other RASopathies indicate that additional pathways downstream of Ras, including PI3K, or pathways that crosstalk with the Ras/MAPK pathway also play a role in amelogenesis. For example, individuals with Tuberous Sclerosis, which is caused by mutations in the AKT targets *TSC1* or *TSC2*, have de-mineralized pits in the enamel surface (54); interestingly, this phenotype is different from the generalized hypo-mineralized enamel defect in CS. These data suggest a role for PI3K in tooth development, and that dysregulation of PI3K signaling may disrupt enamel formation. Further studies of RASopathies, both in terms of clinical phenotyping of patients and through utilization of mouse models for mechanistic studies, will help to dissect the role of Ras signaling in amelogenesis and other tissues.

Because the tooth, like most other organs, develops through reciprocal epithelial–mesenchymal interactions (55, 56), knowledge gained by studying tooth development may be generalizable to other organs. Thus, dissecting the function of the Ras pathway and its many effectors, including MAPK and PI3K, in the teeth of both humans and mice will not only advance our knowledge of signaling in the tooth, but also will provide information on the intricacies of Ras signaling in general, which will in turn advance progress towards treatment of the RASopathies.

MATERIALS AND METHODS

Human subject craniofacial and dental examinations

A total of 41 individuals with a clinical diagnosis of CS were examined during the sixth International Costello Syndrome Conference in Berkeley, California in 2009 (57) and the seventh International Costello Syndrome Family Forum in Chicago, IL in 2011. The diagnosis was confirmed by a board

Downloaded from http://hmg.oxfordjournals.org/ at University of Alabama at Birmingham on December 3, 2013

certified medical geneticist (K.A.R. or O.D.K.) based on clinical features. All 41 participants enrolled in our study were *HRAS* mutation positive. The cohort consisted of 21 males and 20 females. The average age of the cohort was 11 years, with a range of 1–35 years of age. The majority of the cohort reported Caucasian race (80%), but also included were Latino (10%), African (5%), Asian (2%) and Middle Eastern (2%) individuals. A written informed consent was obtained for all subjects. Complete intra- and extra-oral examinations were performed by a licensed dentist (A.F.G.). Examinations included frontal and side view craniofacial photographs, intra-oral photographs, review of radiographs (including panoramic, periapical and bitewing radiographs) and dental records provided by the participant, and alginate dental impressions. Primary teeth exfoliated or naturally lost (not extracted due to caries or to address spacing) were collected from patients. UV images were taken with an Olympus E-620 camera (Center Valley, PA, USA) and a Pentax Ultra-Achromatic Takumar Quartz lens (Denver, CO, USA), which heightened the contrast between areas of mineralized and de-mineralized enamel.

Mouse husbandry and inhibitor treatment

All experiments involving mice were conducted in accordance with protocols approved by the University of California, San Francisco Institutional Animal Care and Use Committee. CS ($Hras^{G12V}$) mice were bred and genotyped as previously described (9). PD0325901 (Pfizer) and GDC0941 (Genentech) were formulated in 0.5% (w/v) (hydroxypropyl)methyl cellulose (HPMT; Sigma, St. Louis, MO). PD0325901 was administered to 12-week-old mice by oral gavage at 12.5 mg/kg and GDC0941 at 75 mg/kg per mouse once per day for 28 days. Minimal side effects, including weight loss, were observed and monitored in mice systemically administered PD0325901 or GDC0941.

μCT and SEM analysis of exfoliated human and mouse teeth

μCT was performed on human teeth and mouse hemi-mandibles. For patient samples, 1 exfoliated primary maxillary central incisor from a CS individual and 1 age-matched control tooth were collected and stored dry at room temperature. For mouse samples, hemi-mandibles from P21 and P70 control and CS ($Hras^{G12V}$) mice were dissected, cleaned of excess tissue and fixed overnight in 4% paraformaldehyde (PFA), followed by dehydration in 70% ethanol. Human and mouse samples were scanned using a micro-focused X-ray tomographic system (MicroXCT-200, Xradia, Pleasanton, CA), at 55 kV and 144 μA. 2000 projection images at an exposure time of 13 s with a linear magnification of 2X were taken. The final pixel size was 20.5 μm. The volume was reconstructed using a back projection filtered algorithm (XRadia). Following reconstruction, 3D image processing and analysis were carried out using MicroView (Version 5.2.2, GE Healthcare, Pittsburgh, PA) and Amira (Version 5.3, Visualization Sciences Group, Burlington, MA) software. A 700 μm transverse section (35 slices) of the incisor, adjacent to the second molar, was used to measure the following parameters: enamel volume and enamel coverage, which is defined by the ratio of enamel area to tooth area.

SEM was performed on exfoliated patient teeth and mouse hemi-mandibles. For patient samples, two exfoliated primary teeth (maxillary central and lateral incisor) from two CS individuals and one exfoliated age-matched control maxillary central incisor were collected and stored dry at room temperature. For mouse samples, hemi-mandibles from 12-week-old control and CS mice were dissected free of soft and connective tissue, fixed in 4% PFA in phosphate buffered saline (PBS) overnight, then dehydrated in a graded ethanol series and dried in a vacuum desiccator. After initial treatment, mouse and human samples were treated the same. Samples were embedded in epoxy resin (resin 105 and hardener 205 at a ratio of 5:1 w/w, WestSystem, Bay City, MI, USA), ground to the desired thickness on a plate grinder (EXAKT 400CS, Norderstedt, Germany) using 800 grit silicon carbide paper and polished with 2000 and 4000 grit silicon carbide paper (Hermes Abrasives, Mississauga, ON, Canada). The exposed tissue was etched with 10% phosphoric acid for 30 s, rinsed with water and dried in a vacuum desiccator. Samples were mounted on SEM stubs with carbon tape, surfaces coated with 7 nm gold using a sputter coating machine (Desk II, Denton Vacuum, Moorestown, NJ, USA) and imaged in a Philips SEM instrument (XL30 ESEM, Philips, Andover, MA, USA) operating at a beam energy of 20 keV in secondary electron or backscatter mode. Images were processed using Adobe Photoshop CS5.1 to adjust upper and lower limits of input levels in grayscale mode and to apply auto balance and auto contrast settings.

Histological analysis of mouse teeth

Postnatal day 2, 21 and 70 CS and control mice were euthanized and mandibles were removed and fixed in 4% paraformaldahyde overnight. Mandibles were then decalcified in 0.5M EDTA for 7–16 days, dehydrated, embedded in paraffin and serially sectioned sagitally or coronally on a Leica microtome at 7 μM. Samples were stained with H&E and imaged at 20× and 40× on a Leica upright microscope. Quantification was done using ImageJ software (58) and statistical significance was determined using Student's *T*-test. Immunohistochemistry (IHC) was also performed following standard protocols using antibodies against GM-130 (Cell Signaling #2296, Danvers, MA, 1:500), amelogenin (Santa Cruz #32892, Dallas, TX, 1:250, USA) and p-ERK (Cell Signaling #9101, 1:250). For proliferation analysis, 10-week control and CS mice were injected intraperitoneally with 1 mg of BrdU 1.5 h prior to euthanization, and IHC was performed using an antibody against BrdU (Abcam #6326, Cambridge, MA, 1:500, USA). The number of nuclei and BrdU cells in the CL and TA region was determined using pixel quantification in Adobe Illustrator.

RNA isolation and qPCR

Mandibular molars were removed from P11 control and CS mandibles in PBS and transferred to Dulbecco's Modified Eagle Medium (DMEM) at 4°C. RNA was extracted from the tissue using the RNeasy mini kit (Qiagen, Germantown, MD, USA). RNA was then quantified using the NanoDrop 2000 (Thermo Scientific, Wilmington, DE, USA), and complementary DNA was made with MMLV Reverse Transcriptase. qPCR were performed using the GoTaq qPCR Master Mix (Promega, Madison, WI) in a Mastercycler Realplex (Eppendorf, Hauppauge, NY, USA). PrimeTime qPCR primers (Integrated DNA Technologies, Coralville, IA, USA) for each of

Downloaded from http://hmg.oxfordjournals.org/ at University of Alabama at Birmingham on December 3, 2013

the genes of interest were used (sequences available upon request). qPCR conditions were as follows: 95°C, 2 min; 40 cycles at 95°C, 15 s; 60°C, 15 s; 68°C, 20 s; followed by a melting curve gradient. Expression levels of the genes of interest were normalized to levels of *L19* and are presented as relative levels to control.

Western blot hybridization

Liver tissue was collected, snap-frozen and homogenized in cell lysis buffer with the addition of a phosphatase inhibitor cocktail. The lysates were cleared by centrifugation and soluble protein quantified by the Bradford method. 2.5 μg of protein was subjected to polyacrylamide gel electrophoresis on a NuPAGE Novex 4–12% Bis-Tris gradient gel (Invitrogen, Grand Island, NY, USA) and transferred to the BVDF membrane. Western blot hybridization was performed using standard protocols. Blots were probed with antibodies to p-MEK1/2 (Cell Signaling #2338), p-ERK (Cell Signaling #9101), total ERK (Cell Signaling #9102), p-AKT (Cell Signaling #9271) and total AKT (Cell Signaling #9272). The antibody to GAPDH (#AM4300, Ambion, Austin, TX) was used as a protein loading control.

SUPPLEMENTARY MATERIAL

Supplementary Material is available at *HMG* online.

ACKNOWLEDGEMENTS

We are grateful to all of the participants in our study and their families and to the Costello Kids Network. We thank Genentech for providing the PI3K inhibitor GDC-0941 and Divya Donthi for technical assistance.

Conflict of Interest statement. None declared.

FUNDING

The authors are funded in part by fellowships and grants from the National Institutes of Health (F30-DE022205 to A.F.G., K99-DE022059 to A.H.J., R01-AR062165 to K.A.R. and R01-DE021420 and DP2-OD00719 to O.D.K.), Canadian Institutes of Health Research (MOP-119310 to B.G.) and Natural Sciences and Engineering Research Council of Canada (RGPIN-403292-11 to B.G.).

REFERENCES

1. Nie, X., Luukko, K. and Kettunen, P. (2006) FGF signalling in craniofacial development and developmental disorders. *Oral Dis.*, **12**, 102–111.
2. Klein, O.D., Minowada, G., Peterkova, R., Kangas, A., Yu, B.D., Lesot, H., Peterka, M., Jernvall, J. and Martin, G.R. (2006) Sprouty genes control diastema tooth development via bidirectional antagonism of epithelial–mesenchymal FGF signaling. *Dev. Cell*, **11**, 181–190.
3. Klein, O.D., Lyons, D.B., Balooch, G., Marshall, G.W., Basson, M.A., Peterka, M., Boran, T., Peterkova, R. and Martin, G.R. (2007) An FGF signaling loop sustains the generation of differentiated progeny from stem cells in mouse incisors. *Development*, **135**, 377–385.
4. Peterkova, R., Churava, S., Lesot, H., Rothova, M., Prochazka, J., Peterka, M. and Klein, O.D. (2009) Revitalization of a diastemal tooth primordium in Spry2null mice results from increased proliferation and decreased apoptosis. *J. Exp. Zoolog.*, **312B**, 292–308.
5. Rauen, K.A. (2007) HRAS and the Costello syndrome. *Clin. Genet.*, **71**, 101–108.
6. Tidyman, W.E. and Rauen, K.A. (2009) The RASopathies: developmental syndromes of Ras/MAPK pathway dysregulation. *Curr. Opin. Genet. Dev.*, **19**, 230–236.
7. Aoki, Y., Niihori, T., Kawame, H., Kurosawa, K., Ohashi, H., Tanaka, Y., Filocamo, M., Kato, K., Suzuki, Y., Kure, S. and Matsubara, Y. (2005) Germline mutations in HRAS proto-oncogene cause Costello syndrome. *Nat. Genet.*, **37**, 1038–1040.
8. Sol-Church, K.S., Stabley, D.L., Demmer, L.A., Agbulos, A., Lin, A.E., Smoot, L., Nicholson, L. and Gripp, K.W. (2009) Male-to-male transmission of Costello syndrome: G12S HRAS germline mutation inherited from a father with somatic mosaicism. *A. J. Med. Genet.*, **149A**, 315–321.
9. Chen, X., Mitsutake, N., LaPerle, K., Akeno, N., Zanzonico, P., Longo, V.A., Mitsutake, S., Kimura, E.T., Geiger, H., Santos, E. *et al.* (2009) Endogenous expression of HrasG12V induces developmental defects and neoplasms with copy number imbalances of the oncogene. *Proc. Natl Acad. Sci.*, **106**, 7979–7984.
10. Estep, A.L., Tidyman, W.E., Teitell, M.A., Cotter, P.D. and Rauen, K.A. (2006) HRAS Mutations in Costello syndrome: detection of constitutional activating mutations in codon 12 and 13 and loss of wild-type allele in malignancy. *Am. J. Med. Genet.*, **140**, 8–16.
11. Gripp, K.W., Lin, A.E., Stabley, D.L., Nicholson, L., Scott, C.I., Doyle, D., Aoki, Y., Matsubara, Y., Zackai, E.H., Lapunzina, P. *et al.* (2005) HRAS Mutation analysis in Costello syndrome: Genotype and phenotype correlation. *Am. J. Med. Genet.*, **140A**, 1–7.
12. Kerr, B., Delrue, M.A., Sigaudy, S., Perveen, R., Marche, M., Burgelin, I., Stef, M., Tang, B., Eden, O.B., O'Sullivan, J. *et al.*. (2006) Genotype–phenotype correlation in Costello syndrome: HRAS mutation analysis in 43 cases. *J. Med. Genet.*, **43**, 401–405.
13. Smith, C.E. and Warshawsky, H. (1975) Cellular renewal in the enamel organ and the odontoblast layer of the rat incisor as followed by radioautography using 3H-thymidine. *Anat. Rec.*, **183**, 523–561.
14. Smith, C.E. and Warshawsky, H. (1977) Quantitative analysis of cell turnover in the enamel organ of the rat incisor. Evidence for ameloblast death immediately after enamel matrix secretion. *Anat. Rec.*, **187**, 63–98.
15. Harada, H., Kettunen, P., Jung, H.S., Mustonen, T., Wang, Y.A. and Thesleff, I. (1999) Localization of putative stem cells in dental epithelium and their association with Notch and FGF signaling. *J. Cell Biol.*, **147**, 105–120.
16. Seidel, K., Ahn, C.P., Lyons, D., Nee, A., Ting, K., Brownell, I., Cao, T., Carano, R.A.D., Curran, T., Schober, M. *et al.* (2010) Hedgehog signaling regulates the generation of ameloblast progenitors in the continuously growing mouse incisor. *Development*, **137**, 3753–3761.
17. Juuri, E., Saito, K., Ahtiainen, L., Seidel, K., Tummers, M., Hochedlinger, K., Klein, O.D., Thesleff, I. and Michon, F. (2012) Sox2+ stem cells contribute to all epithelial lineages of the tooth via Sfrp5+ progenitors. *Dev. Cell*, **23**, 31.
18. Biehs, B., Hu, J.K.-H., Strauli, N.B., Sangiorgi, E., Jung, H., Herber, R.-P., Ho, S., Goodwin, A.F., Dasen, J.S., Capecchi, M.R. *et al.* (2013) Bmi1 represses Ink4a/Arf and Hox genes to regulate stem cells in the rodent incisor. *Nat. Cell Biol.*, **15**, 846–852.
19. Jheon, A.H., Seidel, K., Biehs, B. and Klein, O.D. (2012) From molecules to mastication: the development and evolution of teeth. *Wiley Interdiscip. Rev. Dev. Biol.*, **2**, 165–192.
20. Costello, J.M. (1977) A new syndrome: mental subnormality and nasal papillomata. *Aust. Paediatr. J.*, **13**, 114–118.
21. Teebi, A.S. and Shaabani, I.S. (1993) Further delineation of Costello syndrome. *Am. J. Med. Genet.*, **47**, 166–168.
22. Karlsson, L. (2010) Caries detection methods based on changes in optical properties between healthy and carious tissue. *Int. J. Dent.*, **2010**, 1–9.
23. Resende, R.G., Brito, J.A.R., Souza, L.N., Gomez, R.S. and Mesquita, R.A. (2011) Peripheral calcifying odontogenic cyst: a case report and review of the literature. *Head and Neck Pathol.*, **5**, 76–80.
24. Gibson, C.W., Yuan, Z.A., Hall, B., Longenecker, G., Chen, E., Thyagarajan, T., Sreenath, T., Wright, J.T., Decker, S., Piddington, R. *et al.* (2001) Amelogenin-deficient mice display an amelogenesis imperfecta phenotype. *J. Biol. Chem.*, **276**, 31871–31875.
25. Fukumoto, S. (2004) Ameloblastin is a cell adhesion molecule required for maintaining the differentiation state of ameloblasts. *J. Cell Biol.*, **167**, 973–983.

Downloaded from http://hmg.oxfordjournals.org/ at University of Alabama at Birmingham on December 3, 2013

26. Moffatt, P., Smith, C.E., St-Arnaud, R. and Nanci, A. (2008) Characterization of Apin, a secreted protein highly expressed in tooth-associated epithelia. *J. Cell. Biochem.*, **103**, 941–956.
27. Iwasaki, K., Bajenova, E., Somogyi-Ganss, E., Miller, M., Nguyen, V., Nourkeyhani, H., Gao, Y., Wendel, M. and Ganss, B. (2005) Amelotin—a novel secreted, smeloblast-specific protein. *J. Dent. Res.*, **84**, 1127–1132.
28. Li, C.-Y., Cha, W., Luder, H.-U., Charles, R.-P., McMahon, M., Mitsiadis, T.A. and Klein, O.D. (2012) E-cadherin regulates the behavior and fate of epithelial stem cells and their progeny in the mouse incisor. *Dev. Biol.*, **366**, 357–366.
29. Jheon, A.H., Mostowfi, P., Snead, M.L., Ihrie, R.A., Sone, E., Pramparo, T., Attardi, L.D. and Klein, O.D. (2011) PERP regulates enamel formation via effects on cell–cell adhesion and gene expression. *J. Cell. Sci.*, **124**, 745–754.
30. Hu, J.C.C., Chun, Y.-H.P., Al Hazzazzi, T. and Simmer, J.P. (2007) Enamel formation and Amelogenesis Imperfecta. *Cells Tissues Organs*, **186**, 78–85.
31. Akgül, N., Caglayan, F., Durna, N., Sümbüllü, M.-A., Akgül, H.-M. and Durna, D. (2012) Evaluation of enamel pearls by cone-beam computed tomography (CBCT). *Med. Oral Pathol Oral Cir. Bucal.*, **17**, e218–e222.
32. Takamori, K., Hosokawa, R., Xu, X., Deng, X., Bringas, P. and Chai, Y. (2008) Epithelial fibroblast growth factor receptor 1 regulates enamel formation. *J. Dent. Res.*, **87**, 238–243.
33. Tsuboi, T., Mizutani, S., Nakano, M., Hirukawa, K. and Togari, A. (2003) Fgf-2 regulates enamel and dentine formation in mouse tooth germ. *Calcif. Tissue Int.*, **73**, 496–501.
34. Welch, H.C.E., Coadwell, W.J., Stephens, L.R. and Hawkins, P.T. (2003) Phosphoinositide 3-kinase-dependent activation of Rac. *FEBS Lett.*, **546**, 93–97.
35. Huang, Z., Kim, J., Lacruz, R.S., Bringas, P., Glogauer, M., Bromage, T.G., Kaartinen, V.M. and Snead, M.L. (2011) Epithelial-specific knockout of the Rac1 gene leads to enamel defects. *Eur. J. Oral Sci.*, **119**(Suppl. 1), 168–176.
36. Magudia, K., Lahoz, A. and Hall, A. (2012) K-Ras and B-Raf oncogenes inhibit colon epithelial polarity establishment through up-regulation of c-myc. *J. Cell Biol.*, **198**, 185–194.
37. Yoshimura, T., Arimura, N., Kawano, Y., Kawabata, S., Wang, S. and Kaibuchi, K. (2006) Ras regulates neuronal polarity via the PI3-kinase/Akt/GSK-3β/CRMP-2 pathway. *Bioch. Biophys. Res. Commun.*, **340**, 62–68.
38. Sasaki, A.T., Chun, C., Takeda, K. and Firtel, R.A. (2004) Localized Ras signaling at the leading edge regulates PI3K, cell polarity, and directional cell movement. *J. Cell Biol.*, **167**, 505–518.
39. Liu, H., Radisky, D.C., Wang, F. and Bissell, M.J. (2004) Polarity and proliferation are controlled by distinct signaling pathways downstream of PI3-kinase in breast epithelial tumor cells. *J. Cell Biol.*, **164**, 603–612.
40. Tang, N., Marshall, W.F., McMahon, M., Metzger, R.J. and Martin, G.R. (2011) Control of mitotic spindle angle by the RAS-regulated ERK1/2 pathway determines lung tube shape. *Science*, **333**, 342–345.
41. Steelman, L.S., Pohnert, S.C., Shelton, J.G., Franklin, R.A., Bertrand, F.E. and McCubrey, J.A. (2004) JAK/STAT, Raf/MEK/ERK, PI3K/Akt and BCR-ABL in cell cycle progression and leukemogenesis. *Leukemia*, **18**, 189–218.
42. Meloche, S. and Pouysségur, J. (2007) The ERK1/2 mitogen-activated protein kinase pathway as a master regulator of the G1- to S-phase transition. *Oncogene*, **26**, 3227–3239.
43. Wang, Y., Kim, E., Wang, X., Novitch, B.G., Yoshikawa, K., Chang, L.-S. and Zhu, Y. (2012) ERK Inhibition rescues defects in fate specification of Nf1-deficient neural progenitors and brain abnormalities. *Cell*, **150**, 816–830.
44. Gysin, S., Salt, M., Young, A. and McCormick, F. (2011) Therapeutic strategies for targeting ras proteins. *Genes Cancer*, **2**, 359–372.
45. Rauen, K.A., Banerjee, A., Bishop, W.R., Lauchle, J.O., McCormick, F., McMahon, M., Melese, T., Munster, P.N., Nadaf, S., Packer, R.J. *et al.* (2011) Costello and cardio-facio-cutaneous syndromes: moving toward clinical trials in RASopathies. *Am. J. Med. Genet.*, **157**, 136–146.
46. Jessen, W.J., Miller, S.J., Jousma, E., Wu, J., Rizvi, T.A., Brundage, M.E., Eaves, D., Widemann, B., Kim, M.-O., Dombi, E. *et al.* (2013) MEK Inhibition exhibits efficacy in human and mouse neurofibromatosis tumors. *J. Clin. Invest.*, **123**, 340–347.
47. Chang, T., Krisman, K., Theobald, E.H., Xu, J., Akutagawa, J., Lauchle, J.O., Kogan, S., Braun, B.S. and Shannon, K. (2013) Sustained MEK inhibition abrogates myeloproliferative disease in Nf1 mutant mice. *J. Clin. Invest.*, **123**, 335–339.
48. Nakamura, T., Gulick, J., Pratt, R. and Robbins, J. (2009) Noonan syndrome is associated with enhanced pERK activity, the repression of which can prevent craniofacial malformations. *Proc. Natl Acad. Sci.*, **106**, 15436–15441.
49. Chen, P.-C., Wakimoto, H., Conner, D., Araki, T., Yuan, T., Roberts, A., Seidman, C.E., Bronson, R., Neel, B.G., Seidman, J.G. *et al.* (2010) Activation of multiple signaling pathways causes developmental defects in mice with a Noonan syndrome-associated Sos1 mutation. *J. Clin. Invest.*, **120**, 4353–4365.
50. Anastasaki, C., Rauen, K.A. and Patton, E.E. (2012) Continual low-level MEK inhibition ameliorates cardio-facio-cutaneous phenotypes in zebrafish. *Dis. Model. Mech.*, **5**, 546–552.
51. Niihori, T., Aoki, Y., Narumi, Y., Neri, G., Cavé, H., Verloes, A., Okamoto, N., Hennekam, R.C.M., Gillessen-Kaesbach, G., Wieczorek, D. *et al.* (2006) Germline KRAS and BRAF mutations in cardio-facio-cutaneous syndrome. *Nat. Genet.*, **38**, 294–296.
52. Rodriguez-Viciana, P., Tetsu, O., Tidyman, W.E., Estep, A.L., Conger, B.A., Cruz, M.S., McCormick, F. and Rauen, K.A. (2006) Germline mutations in genes within the MAPK pathway cause Cardio-facio-cutaneous syndrome. *Science*, **311**, 1287–1290.
53. Goodwin, A., Oberoi, S., Landan, M., Charles, C., Groth, J., Martinez, A., Fairley, C., Weiss, L.A., Tidyman, W., Klein, O. *et al.* (2012) Craniofacial and dental development in cardio-facio-cutaneous syndrome: the importance of Ras signaling homeostasis. *Clin. Genet.*, **83**, 539–544.
54. Sparling, J.D., Hong, C.-H., Brahim, J.S., Moss, J. and Darling, T.N. (2007) Oral findings in 58 adults with tuberous sclerosis complex. *J. Am. Acad. Dermatol.*, **56**, 786–790.
55. Tucker, A. and Sharpe, P. (2004) The cutting-edge of mammalian development; how the embryo makes teeth. *Nat. Rev. Genet.*, **5**, 499–508.
56. Jernvall, J. and Thesleff, I. (2000) Reiterative signaling and patterning during mammalian tooth morphogenesis. *Mech. Dev.*, **92**, 19–29.
57. Rauen, K.A., Schoyer, L., McCormick, F., Lin, A.E., Allanson, J.E., Stevenson, D.A., Gripp, K.W., Neri, G., Carey, J.C., Legius, E. *et al.* (2010) Proceedings from the 2009 genetic syndromes of the Ras/MAPK pathway: from bedside to bench and back. *Am. J. Med. Genet.*, **152A**, 4–24.
58. Schneider, C.A., Rasband, W.S. and Eliceiri, K.W. (2012) NIH Image to ImageJ: 25 years of image analysis. *Nat. Methods*, **9**, 671–675.

Downloaded from http://hmg.oxfordjournals.org/ at University of Alabama at Birmingham on December 3, 2013